

Glassy/Ceramic Li₂TiO₃/Li_xB_yO_z Analogous "Solid Electrolyte Interphase" to Boost 4.5 V LiCoO2 in Sulfide-Based All-Solid-State Batteries

Li Feng, Zu-Wei Yin, Chuan-Wei Wang, Zeheng Li,* Shao-Jian Zhang, Peng-Fang Zhang, Ya-Ping Deng, Feng Pan, Bingkai Zhang, and Zhan Lin*

Sulfide-based all-solid-state lithium-ion batteries (ASSLIBs) are the widely recognized approach toward high safety owing to excellent ionic conductivity and nonflammable nature of solid-state electrolytes (SSEs). However, narrow potential window of SSEs brings about serious interfacial parasitic reactions, resulting in fast degradation of the battery. Herein, a glassy/ ceramic analogous solid electrolyte interface (SEI) is constructed on LiCoO₂ (LCO) to enhance interfacial stability between LCO and the Li₁₀GeP₂S₁₂ (LGPS) SSEs. In which, ceramic Li₂TiO₃ guarantees good mechanical toughness of analogous SEI, while glassy LixByOz reinforces the coverage to avoid parasitic reactions. Analogous SEI endows ASSLIBs with excellent cycling and rate performance under an upper charge voltage of 4.3 V with 82.3% capacity retention after 300 cycles at 0.2 C. When pushing charge voltage to 4.5 V, analogous SEI also enables desirable performance with an initial capacity of 172.7 mAh g⁻¹ and long lifespan of 200 cycles at 0.2 C. Both experiments and theoretical computation reveal excellent stability between analogous SEI and LGPS, which endows ASSLIBs with small polarization and improved performance. This work provides an insight on glassy/ceramic analogous SEI strategy to boost the interfacial stability of ASSLIBs.

1. Introduction

Rechargeable lithium-ion batteries (LIBs) have experienced rapid development in the last few decades owing to the overwhelming energy/power density.[1] However, safety issues caused by flammable liquid organic electrolytes seriously hinder their further applications in traditional LIBs.^[2] All-solid-state lithium-ion batteries (ASSLIBs) are regarded as the most promising option to address safety hazard owing to the nonflammable nature of SSEs.^[3] LiCoO₂, a promising oxide cathode in traditional LIBs for portable electronic devices, exhibits a high theoretical specific capacity of >200 mAh g⁻¹ under high upper charge potential (up to 4.5 V vs Li/Li⁺).^[4] Applying LCO as cathode material in ASSLIBs can take both high energy density and good safety into account.^[5] In which, sulfide-based SSEs, e.g., LGPS, could be one of the most desirable choice owing to its ultra-high ionic conductivity

L. Feng

School of Civil and Transportation Engineering Guangdong University of Technology Guangzhou, Guangdong 510006, China

Z.-W. Yin, C.-W. Wang College of Energy Xiamen University Xiamen 361005, China Z.-W. Yin, F. Pan

School of Advanced Materials

Peking University Shenzhen Graduate School

Shenzhen 518055, China

College of Chemical and Biological Engineering **Zhejiang University**

Hangzhou 310027, China E-mail: 11728048@zju.edu.cn

The ORCID identification number(s) for the author(s) of this article

can be found under https://doi.org/10.1002/adfm.202210744.

S.-J. Zhang, B. Zhang, Z. Lin

Guangdong Provincial Key Laboratory of Plant Resources Biorefinery

School of Chemical Engineering and Light Industry

Guangdong University of Technology Guangzhou 510006, China

E-mail: zhanlin@gdut.edu.cn

S.-J. Zhang, B. Zhang, Z. Lin

Jieyang Branch of Chemistry and Chemical Engineering Guangdong

Laboratory

Jieyang 515200, China

Shandong Provincial Key Laboratory/Collaborative Innovation, Center of

Chemical Energy Storage and Novel Cell Technology, School of

Chemistry and Chemical Engineering

Liaocheng University Liaocheng 252000, China

Y.-P. Deng

Department of Chemical Engineering, Waterloo Institute of

Nanotechnology University of Waterloo

Waterloo, ON N2L 3G1, Canada

DOI: 10.1002/adfm.202210744

www.afm-journal.de

1616208.2, 2023, 16, Downloaded from https://advanced.onlinelibtrary.viely.com/doi/10.1002/adf.202210744 by University Town Of Shenzhen, Wiley Online Library on [2311/2025]. See the Terms and Conditions (https://onlinelibrary.wiley.com/terms-and-conditions) on Wiley Online Library or rules of use; OA articles are governed by the applicable Creative Commons Licensea

comparable to traditional liquid electrolyte (10⁻³–10⁻² S cm⁻¹), ^[2,6] However, narrow oxidation limitation of LGPS (1.7–2.1 V vs Li/Li⁺) gives rise to severe parasitic reactions between LCO and LGPS, which increases interfacial resistance and fastens battery degradation.^[7] LCO could enable overwhelming high energy density when extending the upper charge voltage to 4.5 V (vs Li/Li⁺), but it would exacerbate the interfacial stability in turn.^[8] Therefore, overcoming interfacial stability under high voltage is a great challenge for the construction of high-energy ASSLIBs.

Encapsulating chemical/electrochemical inert interface coating layers on LCO is prevailing and efficient method toward stable ASSLIBs. Various interfacial coating layers, including LiNbO₃,^[9] LiAlO₂,^[10] Li₂O-ZrO₂,^[11] Li₂CoTi₃O₈,^[7b] etc., were proposed to address the above-mentioned issues to improve the cycling stability of ASSLIBs. However, current ASSLIBs still suffer from poor capacity delivery, limited cycling life and dissatisfactory rate capability, especially the cycling stability and rate capability of ASSLIBs under higher cut-off charge voltage are still insufficient. To enhance the cycling performance of ASSLIBs under high voltage, interfacial coating layer with high ionic conductivity, low electrical conductivity and excellent high-voltage tolerance is of necessity for the construction of stable cathode/ SSEs interface. [7b,8] In liquid LIBs, solid electrolyte interface (SEI film) plays a decisive role on stabilizing electrode/electrolyte interface by blocking the consecutive electrolyte decomposition. [12] SEI film in LIBs was widely recognized as a mosaic-type structure, which is mainly constituted by various crystal and amorphous components,[13] where the crystal components guarantee the mechanical toughness of SEI and the amorphous components ensure compact SEI structure. [12a,14] These insights on the SEI film present valuable reference on heterogeneous coating layer to overcome interfacial issues between LCO and LGPS in ASSLIBs. Equally important, good lattice matching between LCO and the coating layer can strengthen the affinity, which further contributes to mechanical stability.[4]

Herein, we propose a glassy/ceramic hybrid coating layer on LCO to mimic the traditional SEI structure, which can balance the suppression of interfacial parasitic reactions and the promotion of ionic diffusion at the interface. In which, ceramic lithium-titanium-oxides (Li-Ti-O) exhibits high ionic conductivity and robust crystal structure. Besides, good affinity between LCO and Li-Ti-O well accommodates the internal volume variation of LCO during repeated de-lithiation/lithiation processes. Meanwhile, glassy Li_vB_vO_z ionic conductor applied as the amorphous component is melted and diffused into the gap of ceramic Li-Ti-O coating layer during thermal calcination, which enables a compact coating layer. Thus, a glassy/ceramic Li₂TiO₃/Li_xB_vO_z analogous "SEI" is successfully encapsulated onto the LCO surface, which is confirmed by high-resolution transmission electron microscope (HRTEM) and X-ray adsorption spectroscopy (XAS). Boundary-free interface between LCO and glassy/ ceramic coating layer emphasizes good affinity, which well protects the crystal stability of LCO during cycling. This is strongly evidenced by X-ray photoelectron spectroscopy (XPS) and scanning electron microscope (SEM) results of cycled LCO. Glassy Li_xB_yO_z in coating layer could balance the interfacial lithium distribution owing to the supply of adequate lithium. For comparison, ceramic Li-Ti-O coating layer without glassy component is also prepared on the LCO surface. Experimental and

computational evidence confirm that Li₄Ti₅O₁₂ generates on the LCO surface when lacking glassy Li_xB_yO₇, which would deprive active Li on the LCO surface and lead to the formation of Co₃O₄ boundary layer. Poor ionic conductivity of Co₃O₄ negatively affects the cycling stability and rate performance of ASSLIBs. Theoretical calculations reveal significant stabilization between glassy/ceramic analogous "SEI" with LGPS SSEs, which is also confirmed by XPS with negligible interfacial reactions between LCO and LGPS. The ASSLIBs (as-modified LCO/LGPS/Li-In) with glassy/ceramic analogous "SEI" deliver an excellent cycling stability with an initial specific capacity of 153 mAh g⁻¹ at 0.2 C, and a retentive rate of 82.3% after 300 cycles at the cutoff potential of 4.3 V (vs Li/Li+). The glassy/ceramic analogous "SEI" also delivers an outstanding cycling performance with 80.3% capacity retention for 400 cycles at 0.5 C, and 78.0% capacity retention for 300 cycles at 1 C. At higher upper charge potential of 4.5 V (vs Li/Li⁺), the LCO with glassy/ceramic analogous "SEI" releases high specific capacity of 172.7 mAh g⁻¹ at 0.2 C, and lead to cycling stability up to 200 cycles with 78.8% capacity retention. This work proposes a glassy/ceramic composite analogous "SEI" to endow high-performance ASSLIBs under high upper charge potential, which provides a new analogous "SEI" design principle for stable cathode/SSEs interface construction.

2. Results and Discussion

2.1. Glassy/Ceramic Analogous "SEI" Construction Strategy

Inspired by the SEI film in LIBs, glassy/ceramic analogous "SEI" was fabricated onto the LCO surface to address the interface issues between LCO and LGPS. Li-Ti-O (e.g., Li₄Ti₅O₁₂, Li₂TiO₃, etc.) present superior ionic conductivity and highvoltage tolerance, which can be suitable interface coating layer materials.^[15] Glassy Li₃BO₃ can be melted and diffuse into the gap of TiO2 nanoparticles at high temperature. As shown in Figure 1, during thermal post-treatment, TiO2 transforms into ceramic Li-Ti-O, while melted glassy Li_vB_vO_z diffuses into Li-Ti-O ceramic coating to generate compact and robust glassy/ ceramic analogous "SEI" on the LCO surface. As-fabricated glassy/ceramic analogous "SEI" can enable fast ionic diffusion owing to desirable ionic conductivity of both ceramic Li-Ti-O and glassy Li_vB_vO₂. Besides, compact coating layer also guarantees excellent ability on suppressing parasitic reactions, which improve the cycling stability and rate capability of ASSLIBs.

2.2. Composition and Structure Identification of Glassy/Ceramic Analogous "SEI"

Commercial monocrystalline LCO (bare LCO) displays a spherical morphology with a diameter of \approx 5 μ m (Figure 2a). Highresolution SEM image of bare LCO shows a clean and smooth surface (the inset in Figure 2a). Solid-state mixing method enables uniform TiO₂ nanoparticles to encapsulate LCO with porous surface (donated as TiO₂-LCO) (Figure S1, Supporting Information). The following thermal post-treatment leads to the generation of Ti-based ceramic coating layer with uniform

www.afm-journal.de

16163028, 2023, 16, Downloaded

nlinelibrary.wiley.com/doi/10.1002/adfm.202210744 by University Town Of Shenzhen, Wiley Online Library on [23/11/2025]. See the Terms

of use; OA articles are governed by the applicable Creative Commons

www.advancedsciencenews.com

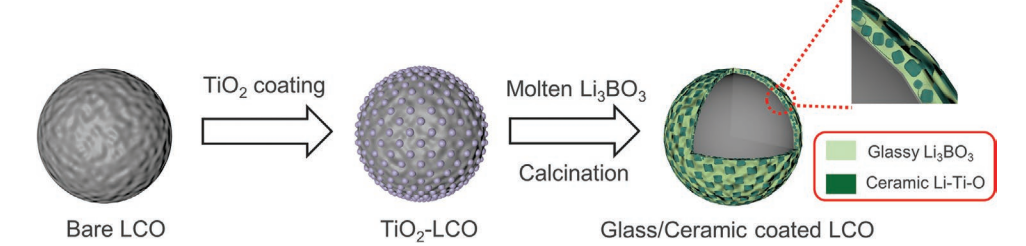


Figure 1. The schematic diagram illustrating the glassy/ceramic analogous "SEI" fabrication on LCO.

and smooth surface on the LCO (donated as ceramic–LCO) (Figure 2b). Electron probe micro-analysis (EPMA) element analysis further highlights a uniform and thin Ti-based coating on the ceramic–LCO surface (Figure S2, Supporting Informa-

tion). After introducing glassy $\text{Li}_x B_y O_z$ in $\text{TiO}_2\text{-LCO}$, a defect-free morphology is achieved after thermal post-treatment (Figure 2c), indicating the glassy $\text{Li}_x B_y O_z$ diffuses into the gaps of Ti-based coating to form glassy/ceramic analogous "SEI"

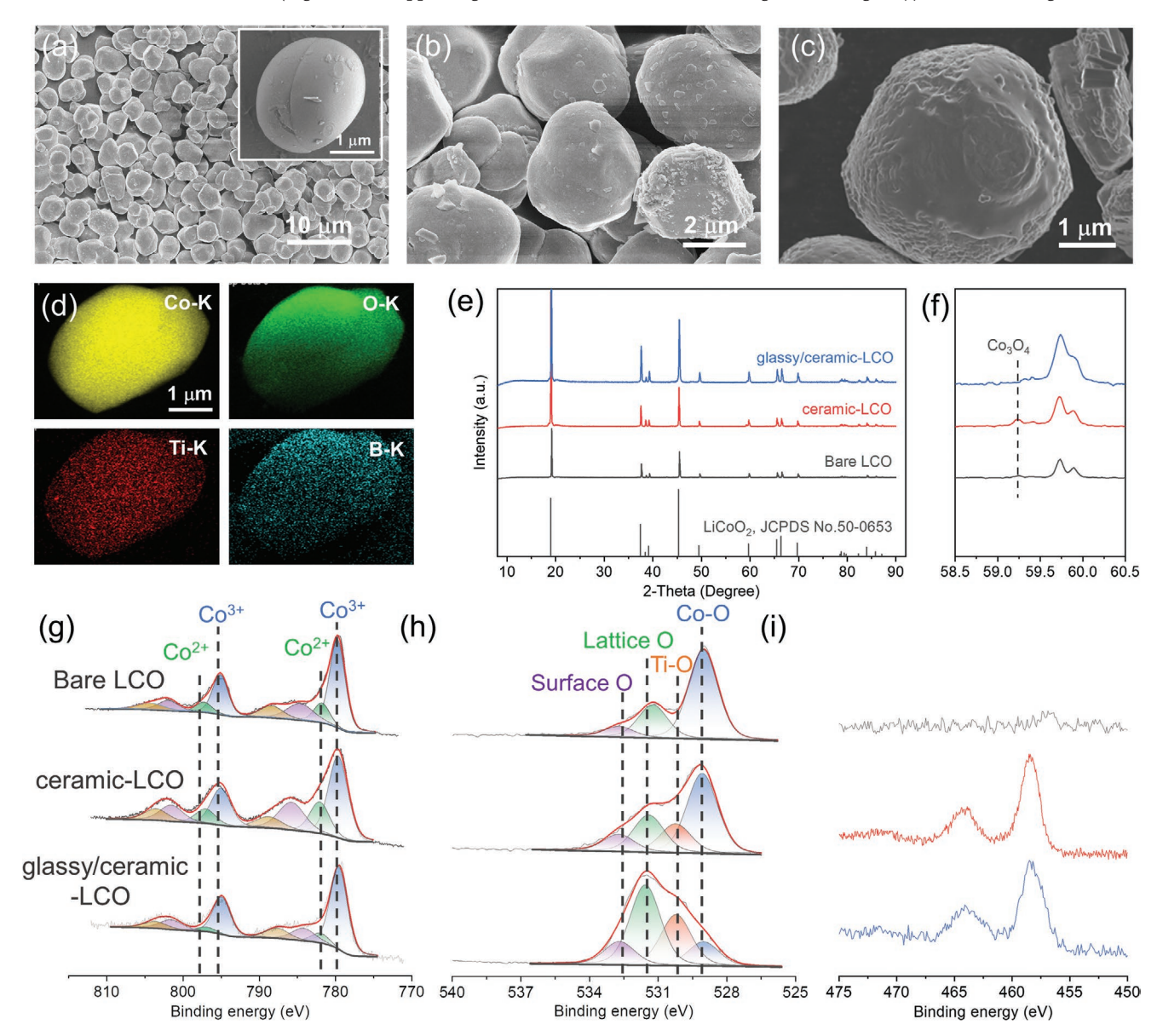


Figure 2. The SEM images of a) bare LCO, b) ceramic–LCO, and c) glassy/ceramic–LCO. d) The TEM-EDS mapping showing the elements distribution of glassy/ceramic–LCO. e) The XRD patterns of ceramic–LCO and glassy/ceramic–LCO. f) Enlarged part of (e) showing the Co_3O_4 formation in c-LCO. The XPS spectra of bare LCO, ceramic–LCO and glassy/ceramic–LCO: g) Co2p, h) O1s, and i) Ti2p.

www.afm-journal.de

1616292, 2023, 16, Downloaded from https://widennced.onlinelibrary.wiely.com/civ/10.1002/aft.f202210744 by University Town Of Shenzhen, Wiley Online Library on [23/11/2025]. See the Terms and Conditions (https://onlinelibrary.wiely.com/terms-and-conditions) on Wiley Online Library or rules of use; OA articles are governed by the applicable Creative Commons License

(denoted as glassy/ceramic–LCO). Transmission electron microscope-energy dispersive spectroscopy (TEM-EDS) mapping analysis reveals uniform distribution of Ti and B elements (Figure 2d), verifying the formation of glassy/ceramic analogous "SEI" on the LCO surface.

The X-ray powder diffraction (XRD) measurements were further carried out to identify the structure of LCO with ceramic coating or glassy/ceramic analogous "SEI". As shown in Figure 2e, compared with bare LCO, ceramic-LCO and glassy/ ceramic-LCO show no obvious structural changes, indicating the analogous "SEI" fabrication has negligible negative impact on LCO crystal. It is worth noting that a new diffraction peak located at 59.2° can be found in ceramic-LCO (Figure 2f), which may be ascribed to spinel Co₃O₄ phase. To confirm that, a control experiment by thermally treating the TiO2 and LCO mixing powder was carried out. Series of diffraction peaks except LCO crystal are detected (Figure S3, Supporting Information), which are identified as spinel Co₃O₄ phase (JCPDS No. 42-1467). This result evidences the formation of spinel Co₃O₄ during the calcination of ceramic-LCO. It is predicted that TiO₂ trends to plunder active Li atoms from bulk LCO to form Li-Ti-O phase, accompanying with Li-free Co₃O₄ formation. However, Li-rich Li_xB_yO_z glass replenishes the Li source during calcination to generate the glassy/ceramic-LCO, preventing the formation of Li-free Co₃O₄ (Figure 2f). Li-free Co₃O₄ exhibits poor electronic/ ionic conductivity, [16] which hinders Li-ion diffusion and further cause negative impacts on the cycling stability and rate capability of ASSLIBs. In contrast, unique glassy/ceramic analogous "SEI on LCO prevents interfacial parasitic reactions between LCO and LGPS. Boundary-free glassy/ceramic analogous "SEI" enables fast ionic diffusion, endowing ASSLIBs with excellent cycling stability, high voltage tolerance, and desirable rate performance. This part will be discussed in detail below.

The XPS spectra were carried out to confirm detailed chemical compositions of coating layers on LCO. Two pairs of split peaks in Co 2p spectra located at 779.3/794.4 and 781.9/796.4 eV are associated with the 2p3/2 and 2p1/2 peaks of Co3+ and Co2+, respectively (Figure 2g). [7b] Bare LCO presents a Co²⁺ fraction of 23.4% on the surface, whilst gradually decreasing with sputtering depth increases, which is contributed to residual Co₃O₄ species on the surface. For the ceramic-LCO, the Co²⁺ on the surface is calculated as 22.1%, and gradually increases to 33.6% at depth of 30 nm below the surface. This result well accords to the formation of Co₃O₄ boundary layer in ceramic-LCO. The applying of glassy phase could suppress the Co₃O₄ formation, as evidenced by steady and low-level Co2+ fractions from the surface to the bulk (Figure 2g; Figure S4, Supporting Information). The B 1s depth profile of glassy/ceramic-LCO was further conducted to reveal the chemical state and distribution of B-related species. As shown in Figure S5 (Supporting Information), the B 1s signal keeps stable with the sputtering depth increase, verifying uniform distribution of B-related species. As compared to the surface observable binding energy shift can be detected, which means the formation of Li₂B₄O₇ species. In addition, oxygen species in bare LCO can be divided into three kinds (Figure 2h): Co−O bonding (≈529 eV), lattice oxygen in LCO crystal (≈531.5 eV), and surface oxygen species (≈533.6 eV). [7b,17] A new peak located at ≈530 eV appears in ceramic-LCO and glassy/ceramic-LCO is ascribed to Li-Ti-O species (Figure 2h).^[18] Obvious Ti signals can be observed in Ti 2p spectra of ceramic–LCO and glassy/ceramic–LCO (Figure 2i), interpreting successful encapsulation of Ti-based coating layer on the LCO surface. The Ti 2p spectra of ceramic–LCO and glassy/ceramic–LCO well matches with Li–Ti–O materials (Li₄Ti₅O₁₄ or Li₂TiO₃), but differs from the TiO₂ material (Figure S6, Supporting Information), verifying the conversion from TiO₂ to Li–Ti–O materials during calcination.

TEM was introduced to explore the microstructures of coating layer. TEM image (Figure S7, Supporting Information) confirms that an inhomogeneous coating layer with a thickness of ≈10 nm is observed on the ceramic–LCO, while a uniform crystalline coating layer with a thickness of ≈15 nm is seen on the glassy/ceramic-LCO. As displayed by HRTEM in Figure 3a-d, the coating layer on the surface of ceramic-LCO is recognized as Li₄Ti₅O₁₂, while a boundary Co₃O₄ layer takes place of the bulk LiCoO2 between bulk LCO and Li₄Ti₅O₁₂ coating layer. Fast Fourier Transform (FFT) of region A in Figure 3a is clearly indexed to the [112] zone of Li₄Ti₅O₁₂ (Figure 3c), while FFT of region B is indexed to the [112] zone of Co₃O₄ (Figure 3d), which indicates a Li₄Ti₅O₁₂/Co₃O₄ heterogeneous structure of coating layer on ceramic-LCO. These results match well with the XRD patterns, further confirm that TiO2 can plunder active Li atoms from bulk LCO to generate Co₃O₄ boundary layer. Scanning transmission electron microscopy (STEM) (Figure 3b) reveals that the interface of regions A and B shows different lattice fringes, in which lattice space $d_1 = 2.95$ Å can be indexed to $\text{Li}_4\text{Ti}_5\text{O}_{12}$ (2–20) and d_2 = 2.85 Å can be indexed to Co_3O_4 (2–20). A lower-magnification STEM image of interface of Li₄Ti₅O₁₂ and Co₃O₄ is displayed in Figure S8 (Supporting Information). Parallel STEM measurement of Li₄Ti₅O₁₂ coating layer also displays spinel phase structure, and the corresponding FFT result further confirms series of diffraction spots associated with the [001] zone of Li₄Ti₅O₁₂ (Figure S9, Supporting Information). The interface of the internal Co₃O₄ boundary layer and bulk LCO was further explored and successfully observed. As shown in Figure S10 (Supporting Information), the region A can be well indexed to the [112] zone of Co₃O₄, while region B can be indexed to the [001] zone of LCO. In the FFT conducted from Figure S10a (Supporting Information), both diffraction spots of Co₃O₄ and LCO are clearly observed, while only diffraction spots of LCO are seen in the bulk LiCoO2 (Figure S10e,f, Supporting Information).

For glassy/ceramic-LCO, the TEM image demonstrates a mosaic-type glassy/ceramic coating layer on bulk LCO (Figure 3e). The FFT of region C and D are indexed to the [111] zone and [110] zone of Li₂TiO₃, respectively (Figure 3g,h), while FFT of region E and F exhibit amorphous structures (Figure S11, Supporting Information). HRTEM of region D displays the (002) orientation of Li₂TiO₃, which has a lattice space of 4.8 Å (Figure 3f). The crystal structure of bulk LCO is shown in Figure S12a (Supporting Information), and the corresponding FFT indexed to the [010] zone is displayed as the inset. The interface of bulk LCO and crystalline Li₂TiO₃ is observed by STEM (Figure S12b, Supporting Information). Due to the different orientations of LCO and Li₂TiO₃, only the [010] zone of LCO is observed. But crystalline Li₂TiO₃ in coating layer matches well with bulk LCO, and no transition phase is observed (Figure S12b, Supporting Information). Based on

16163028, 2023, 16, Downloaded from https://advanced.onlinelibrary.wiley.com/doi/10.1002/adfm.202210744 by University Town Of Shenzhen, Wiley Online Library on [23/11/2025]. See the Terms

nditions) on Wiley Online Library for rules of use; OA articles are governed by the applicable Creative Commons

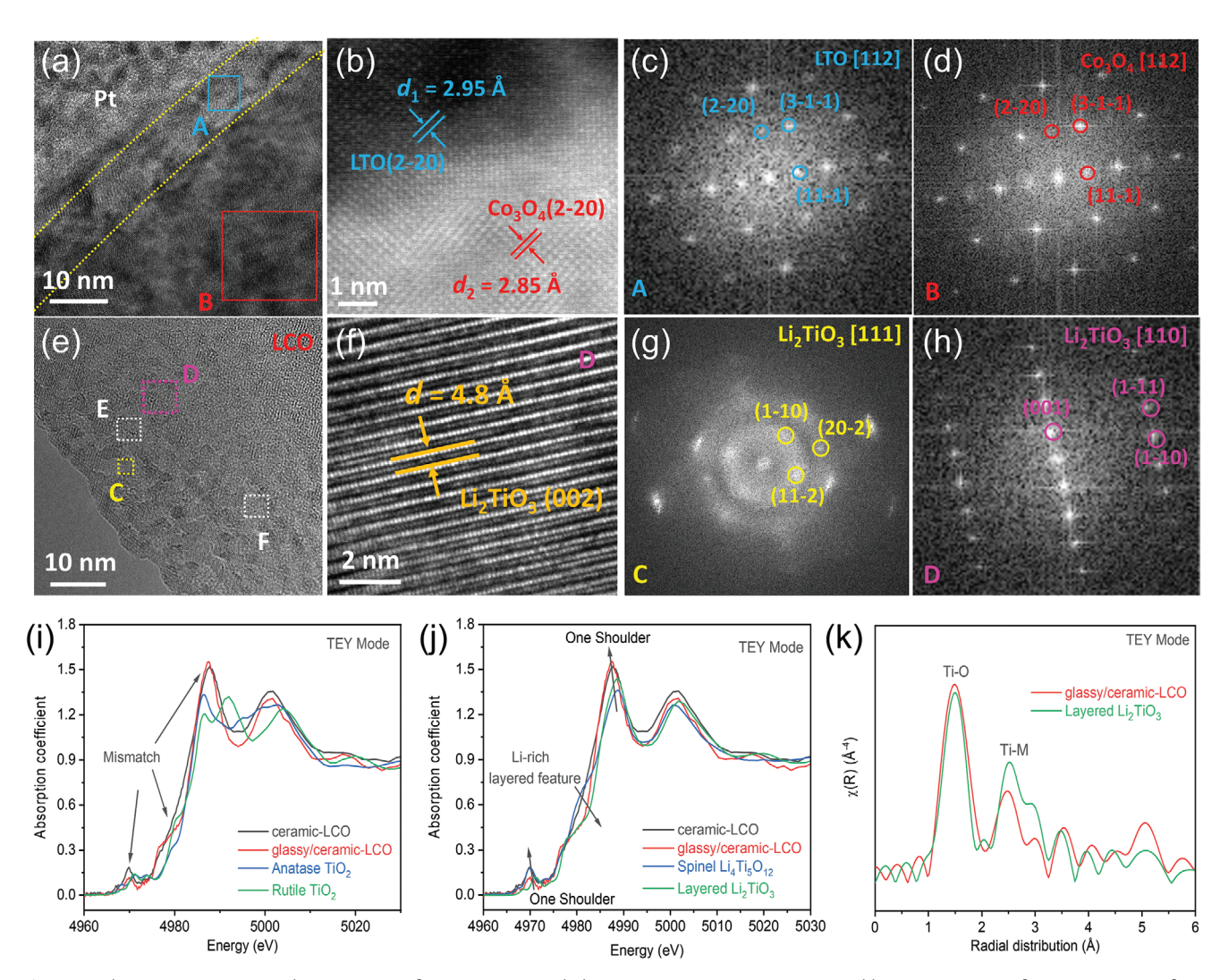


Figure 3. The HRTEM images and XAS spectra of ceramic–LCO and glassy/ceramic–LCO. a) HRTEM and b) STEM images of ceramic–LCO surface. FFT results of c) region A and d) region B marked in (a). e) TEM image of glassy/ceramic–LCO surface. f) The HRTEM image of region D marked in (e). FFT results of g) region C and h) region D marked in (a). i) Ti K-edge XANES spectra of ceramic–LCO, glassy/ceramic–LCO in TEY mode and standard TiO2 (anatase and rutile) samples. j) Ti K-edge XANES spectra of ceramic–LCO, glassy/ceramic–LCO and Li4Ti5O12, Li2TiO3 samples. k) Radial distribution functions (RDF) derived from EXAFS data of glassy/ceramic–LCO and Li2TiO3 standard sample.

uniform distribution of B and O elements and XPS results, the amorphous region is ascribed to glassy $\rm Li_xB_yO_2$. Density functional theory (DFT) computation also provide mutual reaction energies (ΔE) for the formation of glassy/ceramic coating. As shown in Figure S13 (Supporting Information), the ΔE between $\rm Li_4Ti_5O_{12}$ and $\rm Li_3BO_3$ is -0.032 eV atom $^{-1}$, and the phase equilibria is $\rm Li_2TiO_3$, and there is not any reactivity between $\rm Li_2TiO_3$ and $\rm Li_3BO_3$, indicating the introduction of $\rm Li_3BO_3$ would lead to the transformation from $\rm Li_4Ti_5O_{12}$ to $\rm Li_2TiO_3$.

XAS was employed to further investigate the chemical structure of coating layers in ceramic–LCO and glassy/ceramic–LCO. XAS spectrum in total electron yield (TEY) mode reflects the surface information of materials, which is suitable for the characterizations of coating layer. The Ti K-edge XAS spectrum of ceramic–LCO and glassy/ceramic–LCO in TEY mode are demonstrated in Figure S14a (Supporting Information), and Ti K-edge spectrum of TiO₂ (anatase and rutile) is used as com-

parison. The corresponding enlarged image of X-ray adsorption near-edge spectroscopy (XANES) parts (Figure 3i; Figure S15, Supporting Information) shows obvious mismatches among ceramic-LCO and glassy/ceramic-LCO and TiO2 (anatase and rutile). The pre-edge of transition metals (TM) in XAS spectrum presents the hybridization of TM 3d and O 2p orbits, and main peak indicates the electron transfer from TM 1s to 4p orbit.^[20] Previous experimental and simulation results show that TiO₂ (anatase and rutile) have two pre-edge peaks at ≈4970 eV, and their main peaks at ≈4990 eV also split into two peaks. [21] Obviously, only one-shoulder pre-edge at ≈4970 eV and one main peak at ≈4990 eV are found in ceramic-LCO and glassy/ ceramic-LCO, which is coincided with the reported results of Li-Ti-O.[22] The comparison of Ti K-edge XAS spectra of ceramic-LCO and glassy/ceramic-LCO and Li-Ti-O (Li₄Ti₅O₁₂ and Li₂TiO₃) (Figure 3j; Figure S14b, Supporting Information) shows that all of them exhibit one-shoulder pre-edge and

www.afm-journal.de

1616292, 2023, 16, Downloaded from https://widennced.onlinelibrary.wiely.com/civ/10.1002/aft.f202210744 by University Town Of Shenzhen, Wiley Online Library on [23/11/2025]. See the Terms and Conditions (https://onlinelibrary.wiely.com/terms-and-conditions) on Wiley Online Library or rules of use; OA articles are governed by the applicable Creative Commons License

one-shoulder main peak. In the medium part at ≈4980 eV, ceramic-LCO matches well with Li₄Ti₅O₁₂, when glassy/ ceramic-LCO matches well with Li₂TiO₃. The energy positive shift of Li₂TiO₃ at ≈4980 eV is attributed to the Li-rich layered structure, as reported by several researchers.^[23] The radial distribution function (RDF) derived from extend X-ray adsorption fine structure (EXAFS) parts of Ti K-edge spectrum of glassy/ ceramic-LCO (TEY mode) and Li₂TiO₃ are demonstrated in Figure 3k. The radial distribution between 1 and 2 Å presents the Ti-O bonds, and the bond distance between 2 and 3 Å is associated with Ti-M (M = metal) bonds. The RDF of glassy/ ceramic-LCO matches well with Li₂TiO₃. The k²-weighted k space for Ti K-edge of glassy/ceramic-LCO in TEY mode (Figure S16, Supporting Information) matches well with Li₂TiO₃ and shows enough quality for RDF simulation. The Co K-edge XAS spectrum of bare LCO, ceramic-LCO, and glassy/ ceramic-LCO in TEY mode (Figure S17, Supporting Information) show almost the same feature with the same peak energy but a small negative shift at ≈7725 eV. The Co K-edge XAS spectrum of bare LCO, ceramic-LCO, and glassy/ceramic-LCO in total fluorescence yield (FY) mode are shown in Figure S18 (Supporting Information), and the corresponding enlarged XANES part is displayed in Figure S19 (Supporting Information). A 0.24 eV energy negative shift of main peak and a negative energy shift at ≈7725 eV is observed in ceramic–LCO, indicating lower valence state of Co element. It is coincided with lower valence state of Co in Co₃O₄ (+2.67) than that in LiCoO₂ (+3), which have been proved by the XPS results.

Based on the above results, the crystallographic and chemical structure of coating layer in ceramic–LCO and glassy/ceramic–LCO are well defined. The ${\rm TiO_2}$ -only coating layer on LCO derives a ${\rm Li_4Ti_5O_{12}}$ ceramic coating on the LCO surface. While the formation of ${\rm Li_4Ti_5O_{12}}$ plunders active Li atoms from bulk LCO to generate ${\rm Co_3O_4}$ boundary layer, which hinders ionic diffusion due to the ionic insulation of ${\rm Co_3O_4}$. In contract, glassy LBO fulfills the gap of ${\rm TiO_2}$, and form mosaic-type glassy/ceramic coating layer during the formation process of glassy/ceramic–LCO. Moreover, glassy LBO also supplies extra Li source to turn ${\rm TiO_2}$ into layered ${\rm Li_2TiO_3}$ without ${\rm Co_3O_4}$.

2.3. High-Cyclability ASSLIBs Endowed by Glassy/Ceramic Analogous "SEI"

The ASSLIBs were assembled to estimate the effectiveness of glassy/ceramic modification. In which, LGPS was served as SSEs, and Li-In alloy was adopted as anodes. Ceramic-LCO derived from TiO₂ coating with various percentages was first investigated. Briefly, the ceramic–LCO derived from a 0.75 wt.% TiO₂ coated LCO presents a most stable cycling and relatively lower battery polarization (Figure S20, Supporting Information). Closer experiments were carried out to study the optimized LBO contents. With 2 wt.% LBO, the ASSLIBs delivers the most preeminent cycling (Figure S21, Supporting Information). According to these results, optimized TiO₂ and LBO contents were applied in the following discussion.

When the upper voltage of charging is 4.3 V vs Li/Li⁺, the ASSLIBs with bare LCO, ceramic–LCO and glassy/ceramic–LCO deliver initial capacities of 50.3, 148.4, and 154.8 mAh g⁻¹

at 0.2 C, respectively. The polarizations show an obvious trend of bare LCO>ceramic-LCO> glassy/ceramic-LCO. For the bare LCO, the battery suffers from fast degradation and results in very low capacity retention after 50 cycles (9 mAh g⁻¹). This result is ascribed to serious parasitic reactions occurred in LCO/LGPS interface, which is evidenced by huge interface resistance (>10 000 Ω) after cycling (Figure S22, Supporting Information). Prominently performance enhancement is achieved by the ASSLIBs with ceramic-LCO as the cathode. The battery performs much better cyclic stability than the counterpart using bare LCO with a 61.3% capacity retention for 200 cycles (Figure 4b). Outstanding cycling performance is further enhanced by hiring glassy/ceramic coating layer. The battery with glassy/ceramic-LCO delivers a significant capacity retention of 82.3% even after 300 cycles at 0.2 C, indicating that uniform and boundary-free glassy/ceramic coating could prevent interfacial parasitic reactions and strongly enhance the cyclability of ASSLIBs.

As the results mentioned-above, the ceramic-LCO would generate a Li-free Co₃O₄ boundary layer between LCO and Li₄Ti₅O₁₂ coating layer, which show a negative impact on Li ion diffusion. To prove it, the rate performance, together with galvanostatic intermittent titration technique (GITT) and electrochemical impedance spectrum (EIS) were investigated. As shown in Figure 4c, the battery with bare LCO presents a low initial capacity (59.4 mAh g⁻¹) at small current density (0.2 C), suffering from fast capacity fading with current density increasing. Owing to efficient suppression of interfacial parasitic reactions by ceramic coating layer, the capacity delivery of battery significantly increases at small current density (157.0 mAh g^{-1} at 0.2 C, and 127.1 mAh g^{-1} at 0.5 C). However, Li-free Co₃O₄ boundary layer in ceramic-LCO hinders the rate capability of ASSLIBs with only 18 mAh g^{-1} at 2 C. Splendid rate capability can be observed when adopting glassy/ceramic coating layer. Glassy/ceramic coating layer preserves the samelevel discharge capacity compared to that using LCO with ceramic coating layer at small current density. Impressive discharge capacities of 112.8 and 76.2 mAh g^{-1} at 1 and 2 C are available, respectively, proving faster ionic diffusion and more stable interface by glassy/ceramic coating layer.

The GITT was performed to estimate the polarization of ASSLIBs (Figure 4d). Results elucidate that the battery with bare LCO performs a huge polarization at the initial state (0.75 V) and increases sharply to 1.33 V at the end of discharge, indicating a sluggish reaction dynamic when using bare LCO. While ceramic-LCO dramatically reduces the interfacial parasitic reaction and endows a much lower battery polarization than bare LCO. Impressively, a much lower polarization of only 0.21 V is observed in the battery with glassy/ceramic-LCO, and maintains at the low value during discharge, indicating fast ionic diffusion at LCO/LGPS interface by glassy/ceramic coating layer. The interfacial stability was also studied by EIS. As shown in Figure 4e and Figure S23 (Supporting Information), the Nyquist plots of the battery using ceramic-LCO and glassy/ceramic-LCO are provided. The resistance of the cell is divided into four segments: R_{SE} (solid electrolyte resistance), R_{AI} (anode interfacial resistance), R_{CI} (cathode interfacial resistance), and R_{ct} (charge transfer resistance). [24] An equivalent circuit is used for the fitting of Nyquist plots (Figure S24,

www.afm-journal.de

16163028, 2023, 16, Downloaded from https://advanced.onlinelibrary.wiley.com/doi/10.1002/adfm.202210744 by University Town Of Shenzhen, Wiley Online Library on [23/11/2025]. See the Terms

onditions) on Wiley Online Library for rules of use; OA articles are governed by the applicable Creative Commons License

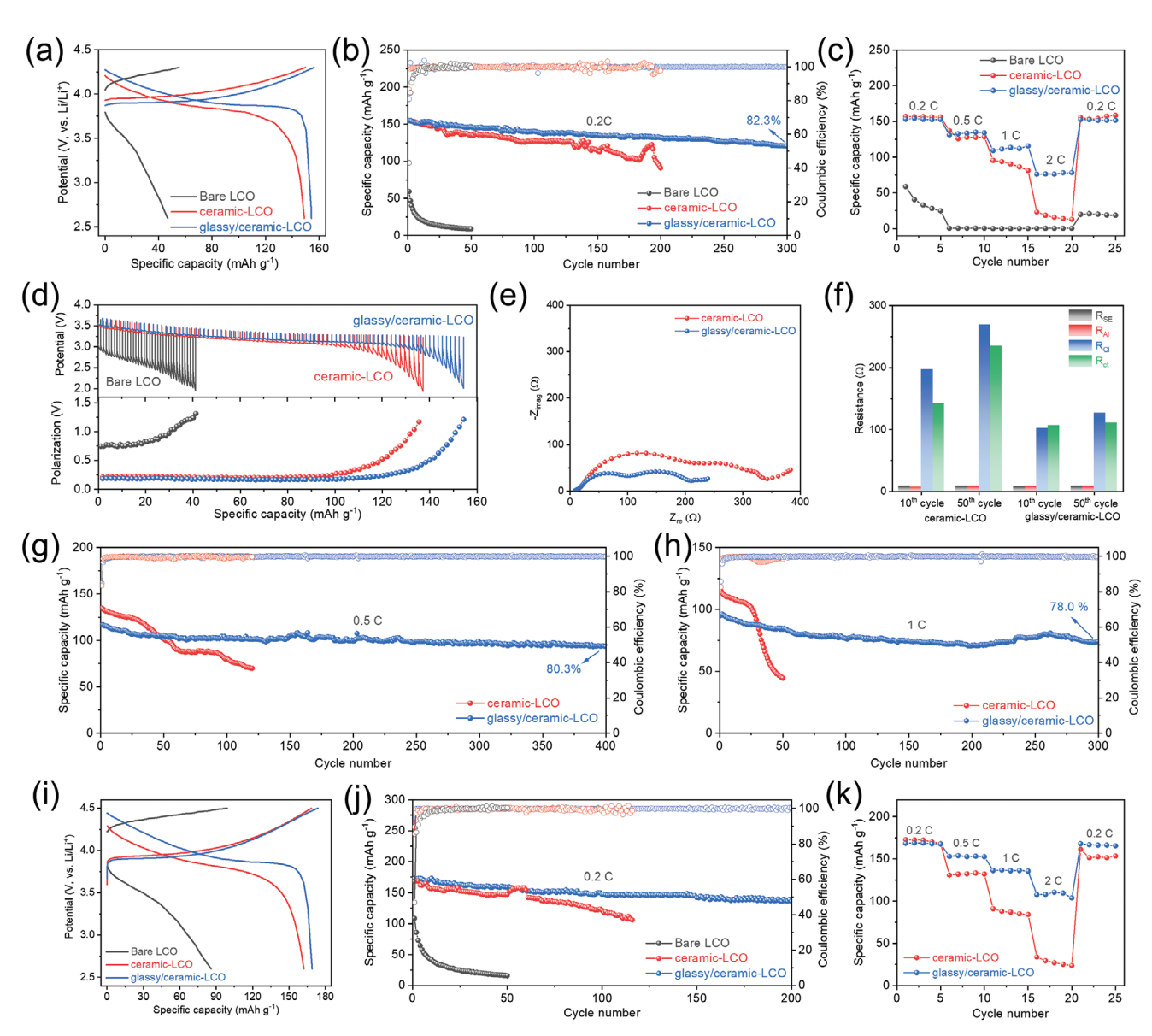


Figure 4. The electrochemical performance of ASSLIBs. a) Cycling performance, b) charge/discharge curves, and c) rate capability of cells with bare LCO, ceramic–LCO, and glassy/ceramic–LCO at a normal charging voltage (4.3 V vs Li/Li+). d) The GITT curves and battery polarization of bare LCO, ceramic–LCO, and glassy/ceramic–LCO. e) Nyquist plots and f) corresponding fitting results of ASSLIBs ceramic–LCO, and glassy/ceramic–LCO after 10 cycles at 0.2 C. The long-term cycling performance of ceramic–LCO, and glassy/ceramic–LCO at g) 0.5 C and h) 1 C rate at a normal charging voltage (4.3 V vs Li/Li+). i) Cycling performance, j) charge/discharge curves and k) rate capability of cells with bare LCO, ceramic–LCO, and glassy/ceramic–LCO at a high voltage (4.5 V vs Li/Li+).

Supporting Information), while the fitting results are concluded in Figure 4f. The R_{CI} and R_{ct} of the battery with ceramic–LCO are 196.5 and 142.6 Ω after 10 cycles at 0.2 C, respectively. These values increase to 269.5 and 234.9 Ω after 50 cycles. When replacing cathode with glassy/ceramic–LCO, much smaller R_{CI} and R_{ct} of 102.2 and 106.2 Ω are achieved after 10 cycles, and only increase slightly after 50 cycles. All the results illustrate glassy/ceramic coating layer significantly suppresses interfacial parasitic reactions, leading to ASSLIBs with outstanding rate performance, low polarization, and small interface resistance.

Long-term cycling stability under high current density was also conducted. As shown in Figure 4g, the battery

with ceramic–LCO performs an initial specific capacity of 134.7 mAh g⁻¹ at 0.5 C but suffers from fast capacity decay in the following cycles. The battery with the glassy/ceramic–LCO exhibits an ultra-stable cycling with a capacity retention as high as 80.4% (94.5 mAh g⁻¹) after 400 cycles. Except that, excellent cycling stability is also endowed by glassy/ceramic coating layer with 96.1 mAh g⁻¹ capacity delivery and 78.0% capacity retention after 300 cycles at 1 C (Figure 4h). These results strongly emphasize the important role of glassy/ceramic coating layer on promoting ionic diffusion and suppressing interfacial parasitic reactions, endowing ASSLIBs with excellent cycling stability and rate capability.

www.afm-journal.de

16163028, 2023, 16, Downloaded from https://advanced.onlinelibrary.wiley.com/doi/10.1002/adfm.202210744 by University Town Of Shenzhen, Wiley Online Library on [23/11/2025]. See the Terms

inditions) on Wiley Online Library for rules of use; OA articles are governed by the applicable Creative Commons

Promoting the upper charge potential of LCO to 4.5 V (vs Li/Li+) can significantly enhance the capacity delivery of LCO. However, high upper charge potential also deteriorates the LCO/LGPS interface stability, which requires coating layer with high oxidation limit. Figure 4i clearly reveals higher discharge capacity when elevating the upper cut-off charge voltage (162.3 mAh g⁻¹ for ceramic-LCO and 170.2 mAh g⁻¹ for glassy/ ceramic-LCO). Huge polarization and low discharge capacity also demonstrate deteriorative LCO/LGPS interface when using bare LCO as cathode, which is also demonstrated by fast degradation on cycling performance at 0.2 C. Remarkable improvement is achieved by ceramic and glassy/ceramic coating layers. The battery using ceramic-LCO preserves 80% capacity retention after 116 cycles, presenting with significant but not satisfactory enhancement by ceramic coating layer (Figure 4j). Impressively, a remarkable discharge capacity of 170.2 mAh g⁻¹ and stable cycling for 200 cycles with 78.8% capacity retention are successfully obtained by using glassy/ceramic-LCO (Figure 4j), highlighting excellent interface stabilization and high-voltage tolerance. Besides, optimized interfacial ionic diffusion by glassy/ceramic coating layer further enables excellent rate performance. As shown in Figure 4k, the capacity of the cell with glassy/ceramic–LCO maintains high retention capacity of 109.7 mAh g⁻¹ at 2 C, which is four-time higher than that with ceramic–LCO (25.1 mAh g⁻¹). These results emphasize that a boundary-free glassy/ceramic coating layer enables excellent interface stability and high interface ionic diffusion, which endows high-performance ASSLIBs with excellent cycling stability, remarkable rate capability, and desirable high voltage tolerance.

2.4. Role of Glassy/Ceramic Analogous "SEI" in Stabilizing LCO/LGPS Interface

Narrow stable potential window of LGPS would give rise to interfacial parasitic reactions, which accumulates ionic insulted compounds in the LCO/LGPS interface. This interfacial issue would block ionic diffusion, resulting in huge interface resistance, high battery polarization as well as battery failure. Herein, XPS spectra were carried out to explore the interfacial stability and identify the parasitic by-products generation in ASSLIBs. Pristine LGPS SSEs presents a pair of split peaks located at 161.0/162.2 eV in S 2p spectra (Figure 5a), which

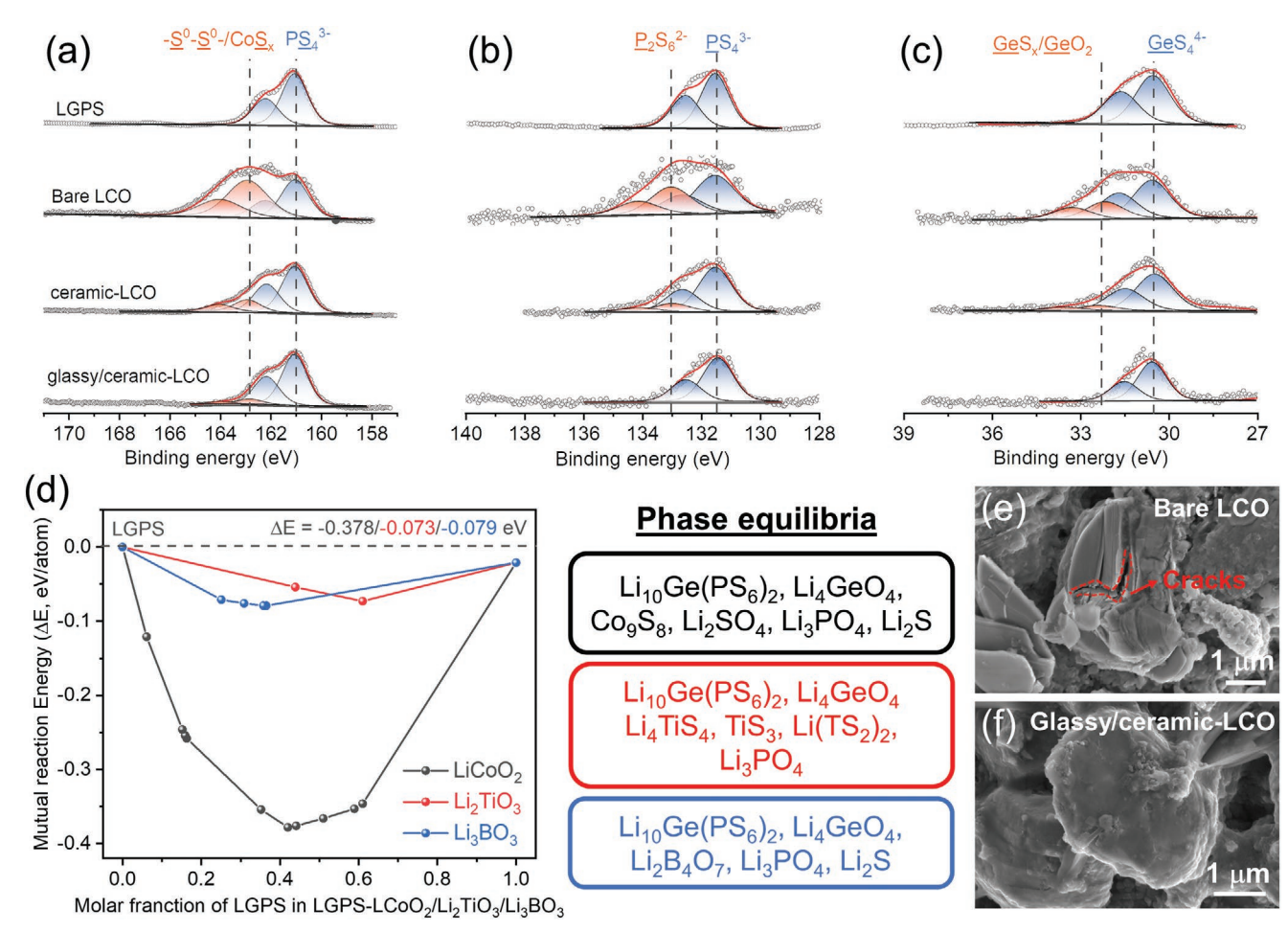


Figure 5. The a) S 2p, b) P 2p, and c) Ge 3d XPS spectra revealing the interfacial parasitic reactions in batteries with bare LCO, ceramic–LCO, and glassy/ceramic–LCO after 10 cycles at 0.2 C. d) Calculated mutual reaction energy of LCO/LGPS, LCO/Li₂TiO₃, and LCO/Li₃BO₃ as a function of the mixing ratio of LGPS and phase equilibria (in box) with largest magnitude of decomposition enthalpy. The SEM images of e) bare LCO and f) glassy/ceramic–LCO after 10 cycles at 0.2 C.



www.afm-journal.de

16163028, 2023, 16, Downloaded from https://advanced.onlinelibrary.wiley.com/doi/10.1002/adfm.202210744 by University Town Of Stenzchen, Wiley Online Library on [23/11/2025]. See the Terms and Conditions (https://doi.org/10.1002/adfm.202210744 by University Town Of Stenzchen, Wiley Online Library on [23/11/2025]. See the Terms and Conditions (https://doi.org/10.1002/adfm.202210744 by University Town Of Stenzchen, Wiley Online Library on [23/11/2025]. See the Terms and Conditions (https://doi.org/10.1002/adfm.202210744 by University Town Of Stenzchen, Wiley Online Library on [23/11/2025]. See the Terms and Conditions (https://doi.org/10.1002/adfm.202210744 by University Town Of Stenzchen, Wiley Online Library on [23/11/2025]. See the Terms and Conditions (https://doi.org/10.1002/adfm.202210744 by University Town Of Stenzchen, Wiley Online Library on [23/11/2025]. See the Terms and Conditions (https://doi.org/10.1002/adfm.202210744 by University Town Of Stenzchen, Wiley Online Library on [23/11/2025]. See the Terms and Conditions (https://doi.org/10.1002/adfm.202210744 by University Town Of Stenzchen, Wiley Online Library on [23/11/2025]. See the Terms and Conditions (https://doi.org/10.1002/adfm.202210744 by University Town Of Stenzchen, Wiley Online Library on [23/11/2025]. See the Terms and Conditions (https://doi.org/10.1002/adfm.202210744 by University Town Of Stenzchen, Wiley Online Library on [23/11/2025]. See the Terms and Conditions (https://doi.org/10.1002/adfm.202210744 by University Town Of Stenzchen, Wiley Online Library on [23/11/2025]. See the Terms and Conditions (https://doi.org/10.1002/adfm.202210744 by University Town Of Stenzchen, Wiley Online Library (https://doi.org/10.1002/adfm.202210744 by University Town Of Stenzchen, Wiley Online Library (https://doi.org/10.1002/adfm.202210744 by University Town Of Stenzchen, Wiley Online Library (https://doi.org/10.1002/adfm.202210744 by University Town Of Stenzchen, Wiley Online Library (https://doi.org/10.1002/adfm.20221074 by University Town Of Stenz

and-conditions) on Wiley Online Library for rules of use; OA articles are governed by the applicable Creative Commons License

are identified as the PS_4^{3-} in LGPS. The PS_4^{3-} also has split peaks sited at 131.6/133.0 eV in P 2p spectra (Figure 5b). In Ge 3d spectra, split peaks at 30.5/31.7 eV can be ascribed to the GeS₄⁴⁻ (Figure 5c).^[25] The PS₄³⁻ oxidation occurs in LCO/LGPS interface in cycled ASSLIBs with bare LCO owing to poor antioxidation of LGPS, which generates the components of oxidized S species (-S⁰-S⁰-) and CoS_x (split peaks at 162.9/164.2 eV in S 2p spectra). [26] Obvious LGPS decomposition is also evidenced by the significant P₂S₆²⁻ species (split peaks located at 133.2/134.3 eV in P 2p spectra) in LCO/LGPS interface.[7b] Besides, the LCO/LGPS interface also has O/S exchange, which is identified from Ge 3d spectra with obvious GeS_x and GeO₂ species (split peaks at 32.2/33.3 eV in Ge 3d spectra) after 10 cycles in the battery using bare LCO.^[27] Ceramic coating layer in ceramic-LCO intercepts direct contact between LGPS and bulk LCO, leading to a suppressive interfacial parasitic reaction. This is supported by declined oxidized S species, CoS_x in S 2p spectra, less P₂S₆²⁻ in P 2p spectra, and suppressive GeS_x/GeO₂ in Ge 3d spectra. However, ceramic coating layer cannot avoid the parasitic reaction, which still accumulate during repeated cycling as well as with shortened cycling life of ASSLIBs. Desirable blockage of interfacial parasitic reactions is observed by hiring glass/ceramic coating layer. To prove it, XPS spectra of interface of glassy/ceramic-LCO was also carried out. Obviously, almost no by-product accumulates at the LCO/LGPS interface, as proved by disappeared oxidized S and CoSx in S 2p spectra. Similar results are also observed in P 2p and Ge 3d spectra with no P₂S₆²⁻ and GeS_x/GeO₂ species, which strongly prove highly stable LCO/LGPS interface constructed by glass/ ceramic coating.

In ASSLIBs, the stability of LCO/LGPS is crucial for cycling performance. Herein, the mutual reaction energy (ΔE) at LCO/LGPS interface was calculated to investigate the strength of interfacial chemical reactions (Figure 5d). The ΔE between LCO and LGPS is as low as -0.378 eV atom⁻¹, accompanying with various decomposition products listed at the right of Figure 5d. Low ΔE means the LCO/LGPS interface is thermodynamically instable, which well accords to poor cycling and rate performance of ASSLIBs with bare LCO. Enhanced cycling and rate performance of ASSLIBs with glassy/ ceramic-LCO originates from the thermo-dynamical stability between glassy/ceramic coating layer with LGPS, which is evidenced by much high ΔE for Li₂TiO₃/LGPS (0.073 eV atom⁻¹) and Li₃BO₃/LGPS (-0.079 eV atom⁻¹). Otherwise, the cycled bare LCO and glassy/ceramic-LCO was also investigated by SEM. As displayed in Figure 5e, cycled bare LCO exhibits damaged morphology with obvious cracks on the LCO particle, which is ascribed to large interior stress resulting from undesirable phase transition during repeated cycling. Cracks generation would expose new fresh LCO surface, leading to unstoppable interface parasitic reaction and fast degradation of electrochemical performance. With glassy/ceramic coating layer, crack-free LCO particles are observed after cycling (Figure 5f), indicating robust glassy/ceramic coating layer well buffers the interior stress. Such comparative results prove that robust glassy/ceramic coating layer thermodynamically suppresses interfacial parasitic reactions, contributing to optimized cycling and rate performance even under higher upper charge potential.

3. Conclusion

In this work, we propose a glassy/ceramic coating on the LCO by mimicking the traditional SEI structure to alleviate the detrimental interfacial parasitic reaction resulted from serious potential mismatching between LCO and LGPS. Comprehensive examination including XPS, TEM, and XAS was applied to demonstrate a hybrid coating layer by combining the ceramic Li₂TiO₃ and glassy Li₃BO₃. Compared with the one with only ceramic coating layer, glassy/ceramic coating layer could eliminate the boundary between bulk LCO and coating layer, leading to robust LCO/LGPS interface and fluent interfacial ionic transportation. Closer examination reveals that glassy/ceramic coating layer is stable enough to suppress the interfacial reactions, which is evidenced by XPS results with less oxidized species in LCO/LGPS interface. Further DFT results also declaims the inherent stability between glassy/ceramic coating layer toward LGPS. As a result, ASSLIBs with glassy/ceramic coated LCO lead to a high specific capacity delivery (154.8 mAh g⁻¹ at 0.2 C), rate capability (76.2 mAh g⁻¹ at 2.0 C), and long-term durability (300 cycles at 0.2 C, 400 cycles at 0.5 C, and 300 cycles at 1.0 C) under a limited upper cut-off voltage of 4.3 V (vs Li/Li⁺). Robust glassy/ceramic coating layer also take effect when upper charge voltage rising to 4.5 V (versus Li/Li+). Outstanding specific capacity of 170.2 mAh g⁻¹ at 0.2 C is performed by LCO with glassy/ceramic coating layer and restrains 80% capacity retention after 200 cycles. This work provided an analogous "SEI" design to pushing ASSLIBs under highvoltage operation, given insights on designing stable interface to achieve ASSLIBs with long cycling and excellent rate capability.

Supporting Information

Supporting Information is available from the Wiley Online Library or from the author

Acknowledgements

L.F., Z.Y., and C.W. contributed equally to this work. The authors are grateful for the financial support provided by the National Natural Science Foundation of China (no. 52000036) and the Science and Technology Planning Project of Guangzhou City (no. 202102021061). The authors also thank the funding supports of National Natural Science Foundation of China (Project 52172190, 52102221, 52150410409, and 52150410411).

Conflict of Interest

The authors declare no conflict of interest.

Data Availability Statement

The data that support the findings of this study are available from the corresponding author upon reasonable request.





16163038, 2023, 16, Downloaded from https://advanced.onlinelibtrary.vilely.com/doi/10.1002/admf.202210744 by University Town Of Shenzhen, Wiely Online Library on [23/11/2025]. See the Terms and Conditions (https://onlinelibtrary.wiely.com/doi/10.1002/admf.202210744 by University Town Of Shenzhen, Wiely Online Library on [23/11/2025]. See the Terms and Conditions (https://onlinelibtrary.wiely.com/doi/10.1002/admf.202210744 by University Town Of Shenzhen, Wiely Online Library on [23/11/2025]. See the Terms and Conditions (https://onlinelibtrary.wiely.com/doi/10.1002/admf.202210744 by University Town Of Shenzhen, Wiely Online Library on [23/11/2025]. See the Terms and Conditions (https://onlinelibtrary.wiely.com/doi/10.1002/admf.202210744 by University Town Of Shenzhen, Wiely Online Library on [23/11/2025]. See the Terms and Conditions (https://onlinelibtrary.wiely.com/doi/10.1002/admf.202210744 by University Town Of Shenzhen, Wiely Online Library on [23/11/2025]. See the Terms and Conditions (https://onlinelibtrary.wiely.com/doi/10.1002/admf.202210744 by University Town Of Shenzhen, Wiely Online Library on [23/11/2025]. See the Terms and Conditions (https://onlinelibtrary.wiely.com/doi/10.1002/admf.202210744 by University Town Of Shenzhen, Wiely Online Library on [23/11/2025]. See the Terms and Conditions (https://onlinelibtrary.wiely.com/doi/10.1002/admf.202210744 by University Town Of Shenzhen, Wiely Online Library on [23/11/2025]. See the Terms and Conditions (https://onlinelibtrary.wiely.com/doi/10.1002/admf.202210744 by University Town Of Shenzhen, Wiely Online Library on [23/11/2025]. See the Terms and Conditions (https://onlinelibtrary.wiely.com/doi/10.1002/admf.202210744 by University Town Of Shenzhen, Wiely Online Library on [23/11/2025]. See the Terms and Conditions (https://onlinelibtrary.wiely.com/doi/10.1002/admf.202210744 by University Town Of Shenzhen, Wiely Online Library on [23/11/2025]. See the Terms and Conditions (https://onlinelibtrary.wiely.com/doi/10.1002/admf.202210744 by University Town O

and-conditions) on Wiley Online Library for rules

of use; OA articles are governed by the applicable Creative Commons

ADVANCED FUNCTIONAL MATERIALS

Keywords

all-solid-state batteries, analogous SEI, glass/ceramic heterostructures, high-voltage LiCoO₂, interfacial stability

Received: September 15, 2022 Revised: November 2, 2022 Published online: January 15, 2023

- [1] a) Z. Lin, T. Liu, X. Ai, C. Liang, Nat. Commun. 2018, 9, 5262;
 b) Z. Li, G. Wu, Y. Yang, Z. Wan, X. Zeng, L. Yan, S. Wu, M. Ling, C. Liang, K. N. Hui, Z. Lin, Adv. Energy Mater. 2022, 12, 2201197.
- [2] E. Quartarone, P. Mustarelli, Chem. Soc. Rev. 2011, 40, 2525.
- [3] a) Y. Guo, S. Wu, Y.-B. He, F. Kang, L. Chen, H. Li, Q.-H. Yang, eScience 2022, 2, 138; b) Y. Wang, Z. Wang, D. Wu, Q. Niu, P. Lu, T. Ma, Y. Su, L. Chen, H. Li, F. Wu, eScience 2022, 2, 537; c) B. Zhang, R. Tan, L. Yang, J. Zheng, K. Zhang, S. Mo, Z. Lin, F. Pan, Energy Stor. Mater. 2018, 10, 139.
- [4] X. Yang, C. Wang, P. Yan, T. Jiao, J. Hao, Y. Jiang, F. Ren, W. Zhang, J. Zheng, Y. Cheng, X. Wang, W. Yang, J. Zhu, S. Pan, M. Lin, L. Zeng, Z. Gong, J. Li, Y. Yang, Adv. Energy Mater. 2022, 12, 2200197.
- [5] L. Fan, S. Wei, S. Li, Q. Li, Y. Lu, Adv. Energy Mater. 2018, 8, 1702657.
- [6] N. Kamaya, K. Homma, Y. Yamakawa, M. Hirayama, R. Kanno, M. Yonemura, T. Kamiyama, Y. Kato, S. Hama, K. Kawamoto, A. Mitsui, *Nat. Mater.* 2011, 10, 682.
- [7] a) F. Han, Y. Zhu, X. He, Y. Mo, C. Wang, Adv. Energy Mater. 2016,
 6, 1501590; b) C.-W. Wang, F.-C. Ren, Y. Zhou, P.-F. Yan, X.-D. Zhou,
 S.-J. Zhang, W. Liu, W.-D. Zhang, M.-H. Zou, L.-Y. Zeng, X.-Y. Yao,
 L. Huang, J.-T. Li, S.-G. Sun, Energy Environ. Sci. 2021, 14, 437.
- [8] L. Wang, X. Sun, J. Ma, B. Chen, C. Li, J. Li, L. Chang, X. Yu, T. S. Chan, Z. Hu, M. Noked, G. Cui, Adv. Energy Mater. 2021, 11, 2100881.
- [9] a) N. Ohta, K. Takada, I. Sakaguchi, L. Zhang, R. Ma, K. Fukuda, M. Osada, T. Sasaki, *Electrochem. Commun.* 2007, 9, 1486;
 b) F. Walther, F. Strauss, X. Wu, B. Mogwitz, J. Hertle, J. Sann, M. Rohnke, T. Brezesinski, J. Janek, *Chem. Mater.* 2021, 33, 2110.
- [10] K. Okada, N. Machida, M. Naito, T. Shigematsu, S. Ito, S. Fujiki, M. Nakano, Y. Aihara, Solid State Ionics 2014, 255, 120.
- [11] Y.-G. Lee, S. Fujiki, C. Jung, N. Suzuki, N. Yashiro, R. Omoda, D.-S. Ko, T. Shiratsuchi, T. Sugimoto, S. Ryu, J. H. Ku, T. Watanabe, Y. Park, Y. Aihara, D. Im, I. T. Han, Nat. Energy 2020, 5, 299.
- [12] a) K. Xu, Chem. Rev. 2004, 104, 4303; b) T. Liu, Q. Chu, C. Yan, S. Zhang, Z. Lin, J. Lu, Adv. Energy Mater. 2018, 9, 1802645.
- [13] E. Peled, D. Golodnitsky, G. Ardel, J. Electrochem. Soc. 1997, 144, L208.
- [14] J. Tan, J. Matz, P. Dong, J. Shen, M. Ye, Adv. Energy Mater. 2021, 11, 2100046.

- [15] a) J. Wolfenstine, J. L. Allen, J. Power Sources 2008, 180, 582;
 b) X. Wu, Z. Wen, X. Xu, J. Han, Solid State Ionics 2008, 179, 1779;
 c) C.-W. Wang, Y. Zhou, J.-H. You, J.-D. Chen, Z. Zhang, S.-J. Zhang, C.-G. Shi, W.-D. Zhang, M.-H. Zou, Y. Yu, J.-T. Li, L.-Y. Zeng, L. Huang, S.-G. Sun, ACS Appl. Energy Mater. 2020, 3, 2593.
- [16] Y. Ji, J. A. Kilner, M. F. Carolan, J. Eur. Ceram. Soc. 2004, 24, 3613.
- [17] J. Zhang, P. Tang, T. Liu, Y. Feng, C. Blackman, D. Li, J. Mater. Chem. A 2017, 5, 10387.
- [18] J. Mosa, J. F. Vélez, J. J. Reinosa, M. Aparicio, A. Yamaguchi, K. Tadanaga, M. Tatsumisago, J. Power Sources 2013, 244, 482.
- [19] a) S. L. M. Schroeder, G. D. Moggridge, R. M. Ormerod, T. Rayment, R. M. Lambert, Surf. Sci. 1995, 324, L371; b) J. Wang, S.-J. Kim, J. Liu, Y. Gao, S. Choi, J. Han, H. Shin, S. Jo, J. Kim, F. Ciucci, H. Kim, Q. Li, W. Yang, X. Long, S. Yang, S.-P. Cho, K. H. Chae, M. G. Kim, H. Kim, J. Lim, Nat. Catal. 2021, 4, 212.
- [20] a) P. Zimmermann, S. Peredkov, P. M. Abdala, S. DeBeer, M. Tromp,
 C. Müller, J. A. van Bokhoven, *Coord. Chem. Rev.* 2020, 423, 213466;
 b) R. Zimmermann, R. Claessen, F. Reinert, P. S. Steiner, S. Hüfner,
 J Phys Condens Matter 1998, 10, 5697.
- [21] T. C. Rossi, D. Grolimund, M. Nachtegaal, O. Cannelli, G. F. Mancini, C. Bacellar, D. Kinschel, J. R. Rouxel, N. Ohannessian, D. Pergolesi, T. Lippert, M. Chergui, *Phys. Rev. B* 2019, 100, 245207.
- [22] X. Yu, H. Pan, W. Wan, C. Ma, J. Bai, Q. Meng, S. N. Ehrlich, Y. S. Hu, X. Q. Yang, *Nano Lett.* 2013, 13, 4721.
- [23] a) H. Koga, L. Croguennec, M. Ménétrier, P. Mannessiez, F. Weill, C. Delmas, S. Belin, J. Phys. Chem. C 2014, 118, 5700; b) Z.-W. Yin, Z.-G. Wu, Y.-P. Deng, T. Zhang, H. Su, J.-C. Fang, B.-B. Xu, J.-Q. Wang, J.-T. Li, L. Huang, X.-D. Zhou, S.-G. Sun, J. Phys. Chem. C 2016, 120, 25647.
- [24] a) X. Li, H. Guan, Z. Ma, M. Liang, D. Song, H. Zhang, X. Shi, C. Li, L. Jiao, L. Zhang, J. Energy Chem. 2020, 48, 195; b) G. Oh, M. Hirayama, O. Kwon, K. Suzuki, R. Kanno, Chem. Mater. 2016, 28, 2634.
- [25] S. Deng, X. Li, Z. Ren, W. Li, J. Luo, J. Liang, J. Liang, M. N. Banis, M. Li, Y. Zhao, X. Li, C. Wang, Y. Sun, Q. Sun, R. Li, Y. Hu, H. Huang, L. Zhang, S. Lu, J. Luo, X. Sun, *Energy Stor. Mater.* 2020, 27 117
- [26] a) F. Zhao, Y. Zhao, J. Wang, Q. Sun, K. Adair, S. Zhang, J. Luo, J. Li, W. Li, Y. Sun, X. Li, J. Liang, C. Wang, R. Li, H. Huang, L. Zhang, S. Zhao, S. Lu, X. Sun, Energy Stor. Mater. 2020, 33, 139; b) S. Deng, Q. Sun, M. Li, K. Adair, C. Yu, J. Li, W. Li, J. Fu, X. Li, R. Li, Y. Hu, N. Chen, H. Huang, L. Zhang, S. Zhao, S. Lu, X. Sun, Energy Stor. Mater. 2021, 35, 661.
- [27] C. Wang, S. Hwang, M. Jiang, J. Liang, Y. Sun, K. Adair, M. Zheng, S. Mukherjee, X. Li, R. Li, H. Huang, S. Zhao, L. Zhang, S. Lu, J. Wang, C. V. Singh, D. Su, X. Sun, Adv. Energy Mater. 2021, 11, 2100210.